
01 Jul 2022

Effect of Grain Size on the Irradiation Response of Grade 91 Steel Subjected to Fe Ion Irradiation at 300 °C

Jiaqi Duan

Haiming Wen

Missouri University of Science and Technology, wenha@mst.edu

Li He

Kumar Sridharan

et. al. For a complete list of authors, see https://scholarsmine.mst.edu/matsci_eng_facwork/2880

Follow this and additional works at: https://scholarsmine.mst.edu/matsci_eng_facwork



Part of the [Materials Science and Engineering Commons](#)


Recommended Citation

J. Duan et al., "Effect of Grain Size on the Irradiation Response of Grade 91 Steel Subjected to Fe Ion Irradiation at 300 °C," *Journal of Materials Science*, vol. 57, no. 28, pp. 13767 - 13778, Springer, Jul 2022. The definitive version is available at <https://doi.org/10.1007/s10853-022-07480-6>

This Article - Journal is brought to you for free and open access by Scholars' Mine. It has been accepted for inclusion in Materials Science and Engineering Faculty Research & Creative Works by an authorized administrator of Scholars' Mine. This work is protected by U. S. Copyright Law. Unauthorized use including reproduction for redistribution requires the permission of the copyright holder. For more information, please contact scholarsmine@mst.edu.



Effect of grain size on the irradiation response of grade 91 steel subjected to Fe ion irradiation at 300 °C

Jiaqi Duan^{1,2}, Haiming Wen^{1,3,*} , Li He⁴, Kumar Sridharan⁴, Andrew Hoffman³,
Maalavan Arivu¹, Xiaoqing He^{5,6}, Rinat Islamgaliev⁷, and Ruslan Valiev⁷

¹Department of Materials Science and Engineering, Missouri University of Science and Technology, Rolla, MO 65409, USA

²Warwick Manufacturing Group, The University of Warwick, Coventry CV4 7AL, UK

³Department of Nuclear Engineering and Radiation Science, Missouri University of Science and Technology, Rolla, MO 65409, USA

⁴Departments of Engineering Physics and Materials Science & Engineering, University of Wisconsin, Madison, WI 53706, USA

⁵Electron Microscopy Core Facilities, University of Missouri, Columbia, MO 65211, USA

⁶Department of Mechanical and Aerospace Engineering, University of Missouri, Columbia, MO 65211, USA

⁷Institute of Physics of Advanced Materials, Ufa State Aviation Technical University, Ufa 450008, Russia

Received: 2 May 2022

Accepted: 22 June 2022

Published online:

14 July 2022

© The Author(s), under
exclusive licence to Springer
Science+Business Media, LLC,
part of Springer Nature 2022

ABSTRACT

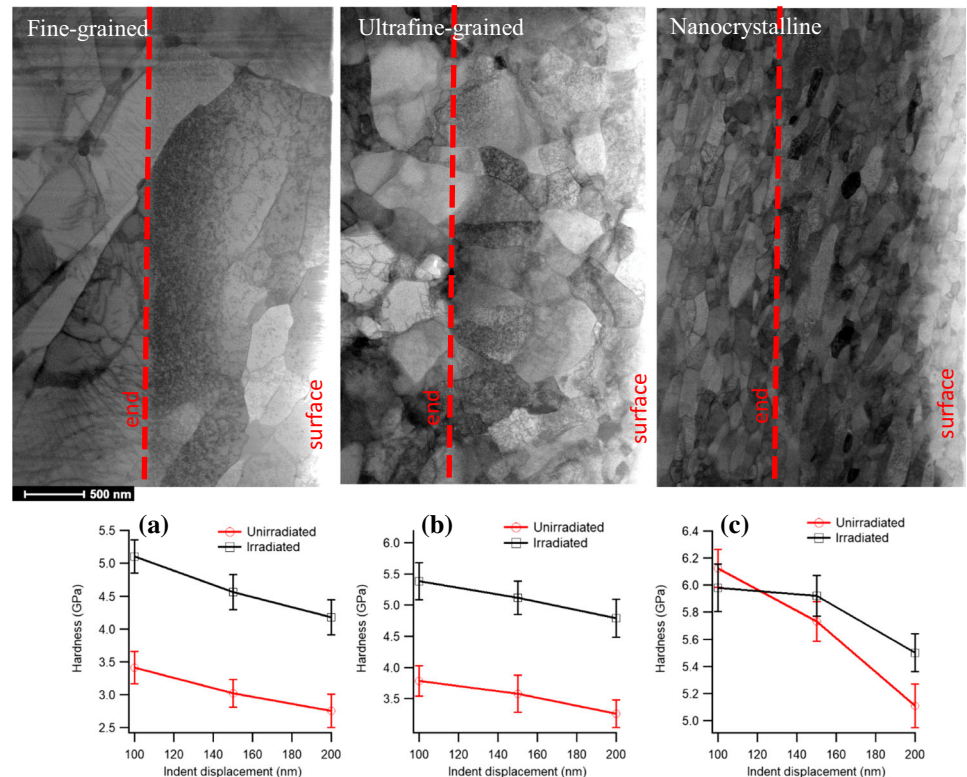
Irradiation using Fe ion at 300 °C up to 100 dpa was carried out on three variants of Grade 91 (G91) steel samples with different grain size ranges: fine-grained (FG, with blocky grains of a few micrometers long and a few hundred nanometers wide), ultrafine-grained (UFG, grain size of ~ 400 nm) and nanocrystalline (NC, lath grains of ~ 200 nm long and ~ 80 nm wide). Electron microscopy investigations indicate that NC G91 exhibit higher resistance to irradiation-induced defect formation than FG and UFG G91. In addition, nano-indentation studies reveal that irradiation-induced hardening is significantly lower in NC G91 than that in FG and UFG G91. Effective mitigation of irradiation damage was achieved in NC G91 steel in the current irradiation condition.

Handling Editor: Naiqin Zhao.

Address correspondence to E-mail: wenha@mst.edu

<https://doi.org/10.1007/s10853-022-07480-6>

GRAPHICAL ABSTRACT



Introduction

Ferritic–martensitic (FM) steels such as Grade 91 (G91) are excellent candidates for fuel cladding and structural materials for advanced fast reactors due to their good thermo-mechanical properties at 400–550 °C and reduced void swelling compared to austenitic stainless steels [1–5]. G91 steel has also been suggested as potential structural material for light water reactor (LWR) core internals. Structural materials and fuel cladding in advanced fast reactors will be subject to high irradiation doses. Life extension of LWRs and development of advanced fast reactors requires steels with enhanced irradiation tolerance and higher mechanical strength [4, 6]. However, FM steels suffer profusely from pronounced hardening and embrittlement when they are irradiated at low temperatures [1, 7]. Konstantinović MJC, et al. [7] reported the mechanical properties of T91 subjected to 0.8–3.9 displacements per atom

(dpa) at 250–350 °C, and they found significant irradiation hardening and decrease of elongation in the materials. At higher temperatures, softening was found in a T91 steel at doses above 0.5 dpa, due to the fast coalescence of dislocation loops [8]. To achieve enhanced irradiation tolerance and higher strength, currently used/considered steels may be processed by advanced manufacturing techniques to improve their performance through microstructural engineering at relatively low cost. Equal-channel angular pressing (ECAP) and high-pressure torsion (HPT) produce UFG and NC, respectively, metals and alloys through application of severe plastic deformation. The applications of ECAP and HPT to G91 steel for grain refinement have been reported [9–11]. Nanostructured (UFG and NC) steels possess dramatically higher strength than their conventional FG (grain diameter > 1 μm) counterparts, owing to significant grain boundary (GB) strengthening. Meanwhile, GBs can also significantly enhance irradiation tolerance of

the materials by serving as sinks or recombination centers for radiation-induced defects [12–14].

In-situ ion irradiation experiments provided the direct evidence of GBs absorbing individual loops and dislocation segments in nanocrystalline Ni when the material was irradiated by Kr ions of 1 MeV at room temperature [14]. In addition, molecular dynamic (MD) simulations were used to determine the mechanism of the interactions between the defects and GBs at the atomic level. The MD simulations of body-centered cubic Fe by Chen, et al. [15] suggested that irradiation-induced defects can either migrate via the bulk chain of defects from matrix to GBs or via GB chain of defects until they are annihilated. F/M T91 steel processed by ECAP was irradiated by Fe ions at 450 °C up to ~ 150 dpa, and the UFG sample showed a lower defect density and smaller swelling rate than the coarse-grained counterpart [16].

Although the defect-GB interactions have been well studied, only very limited investigations exist on irradiation of nanostructured steels, and their performance under irradiation at relevant reactor operating temperatures remains unclear. Notably, previous reports on irradiation study of NC steels have been rare. This work studied the irradiation performance of G91 steel with different grain size ranges down to the nanometer regime and enhanced our understanding of irradiation effects in these materials. The establishment of irradiation performance of nanostructured F/M steels with appealing properties will impact the life extension of current reactors and the development of advanced reactors.

Experimental

A hot rolled G91 steel of the composition Fe–8.38Cr–0.9Mo–0.2 V–0.06Nb–0.17Ni–0.43Mn–0.1C–0.03 N (in wt.%) was normalized at 1050 °C for one hour and then quenched in oil, followed by tempering at 800 °C for one hour and subsequent air cooling. After tempering the G91 steel samples were processed by ECAP and HPT, respectively. The processing details of ECAP and HPT and the resultant microstructures were documented in our previous studies [9–11]. The G91 after tempering consists of blocky grains of a few micrometers long and a few hundred nanometers wide. Grains were successfully refined to sub-micrometer and nanometer range after ECAP and HPT,

respectively. Therefore, the as-tempered, as-ECAP, and as-HPT G91 samples are designated as FG, UFG and NC G91, respectively.

Samples of $5 \times 5 \times 1$ mm were cut from as tempered, as-ECAP and as-HPT G91, respectively. Prior to irradiation, samples were mechanically polished with 0.02 μm colloidal silica in the final stage. Samples were irradiated by 3.7 MeV Fe^{2+} ions using a NEC 1.7 MV tandem accelerator with a rastered beam at the University of Wisconsin Ion Beam Laboratory. Rastered beam was applied for irradiating a relatively large area over multiple samples. Rastered beam has been reported to suppress cavity swelling. For ferritic and ferritic-martensitic steels peak void swelling temperature of 450–480 °C was reported under ion irradiations [17–19].

The ion energy was chosen for two reasons: (1). implantation depth: the flat region of damage profile (half of the dpa peak depth) is about 0.5 μm in depth. Studies have indicated that the surface effect on defects can extend to a depth of 0.2–0.3 μm [20, 21]. The damage flat region is outside of the expected surface effect depth. 2). The accelerating capability: although the maximum accelerating voltage for Fe^{2+} is $3 \times 1.7 = 5.1$ MV, 1.23 MV was operated for achieving a stable ion beam current. An irradiation temperature of 300 °C was selected considering that the temperature regime important for LWR operation is between 280 and 320 °C and that FM as nuclear material could suffer from irradiation-induced embrittlement and hardening at low temperatures. However, at this temperature, swelling is not expected to be significant. Ion fluence was 9.73×10^{16} ion/ cm^2 , and the dose rate was 5.2×10^{12} ion/ cm^2/s . Temperature was monitored continuously throughout irradiation from two thermocouples attached to the opposite corners of the sample irradiation stage. The average temperature was measured as 300 ± 5 °C. Local dose and implanted Fe ion concentration in the samples were calculated using the Kinchin-Pease model with full cascade in the Stopping and Range of Ions in Matter (SRIM) software [22–24], Fig. 1. A displacement threshold energy of 40 eV and a density of 8.47×10^{22} atoms/ cm^3 for G91 was used in the calculation. The middle range dose rate was about 2×10^{-3} dpa/s. Studies have recommended Kinchin-Pease model for comparison of ion and neutron irradiation data while full cascade

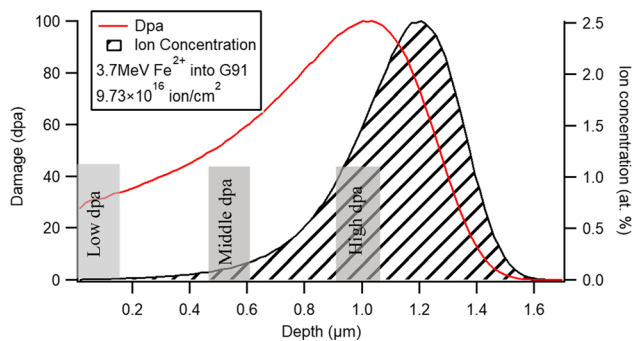


Figure 1 SRIM calculated damage and implanted ion concentration profile in G91 steel. The depth for evaluation is highlighted.

calculation is recommended with multicomponent target materials [23].

Cross-sectional TEM samples were prepared by focused ion beam (FIB) using a dual-beam FEI Helios Nanolab. The voltage of the ion beam for early thinning was 30 keV, and it was reduced to 5 keV as the foil became thinner. For final thinning at thickness of 100–150 nm, a voltage of 5–2 keV was used, so that the damage from FIB could be minimized. Three regions in each sample were examined, as marked in the damage & implantation-depth profile in Fig. 1, i.e. low, middle and high displacement per atom (dpa) regions. The TEM sample thicknesses were measured by electron energy loss spectroscopy (EELS) using a Gatan Quantum image filter on a FEI Tecnai G2 FEG TEM operated with a 300 keV electron beam. Measurements were carried out in the regions of interest. The log-ratio method was used to calculate the thickness of the sample relative to the inelastic mean free path (IMFP), and the measurement errors were assumed $\pm 20\%$ [25, 26]. The TEM samples are wedge-shaped. The thickness variations from the low to high dpa for the FG, UFG, and NC G91 TEM samples are 104–135 nm, 128–159 nm and 140–155 nm, respectively. Scanning transmission electron microscopy (STEM) observations were performed in annular bright field mode under [110] or [111] zone to capture the total loop and line dislocation density. The semi-convergence angle was 24.5 mrad. The collection angle was 6–13 mrad. All g vectors contributed to the images. The defects were manually measured with ImageJ and only the black spots > 1 nm were considered. Under-focus observations were carried out in each specimen to analyze the voids produced by ion irradiation. Carbon contamination was not measured in this study.

Nano hardness was measured with a Hysitron TI-950 tribointender and a cube corner probe in the displacement control mode. Ten indents were carried out in the un-irradiated (unexposed to ion beam) regions and in the irradiated regions, respectively, of each sample at displacements of 100, 150 and 200 nm.

Results

Microstructure

The microstructures of FG, UFG and NC G91 steels are presented in Fig. 2, with a dash line separating the irradiated and un-irradiated regions in each image. The microstructure of the FG G91 consists of typical tempered martensitic blocky grains. Carbides are observed along the lath boundaries. For the UFG G91, the microstructure is characterized by equiaxed grains with an average size of ~ 400 nm. The NC G91 exhibits lath grains elongated along the shear direction. The average width and length of those lath grains are 80 nm and 200 nm, respectively. In each of the G91 steel samples, the grains in the irradiated and un-irradiated regions have comparable sizes, indicating that the current irradiation condition did not lead to grain coarsening. However, grains in NC G91 (both in the irradiated and un-irradiated regions) coarsened slightly during the irradiation experiment due to the thermal effect [11]. FG and UFG G91 show abundant irradiation-induced features, such as dislocation loops and dislocation lines, in the irradiated regions. For the NC G91, it is difficult to observe the

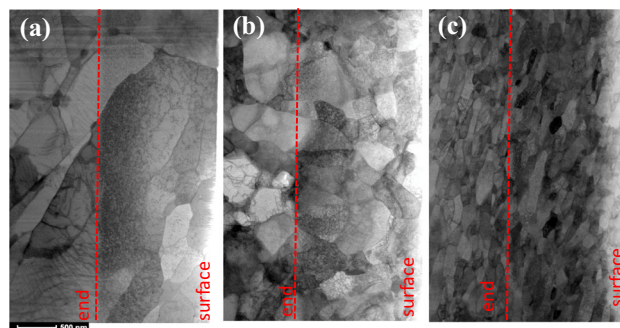


Figure 2 Cross-section STEM micrographs showing the microstructure of FG (a), UFG (b) and NC (c) G91 steel samples subjected to Fe ion irradiation up to 100 dpa at 300 °C. The irradiation affected zone is highlighted in each graph (from surface to the end line).

irradiation-induced defects at the magnification in Fig. 2c.

Figure 3 displays bright-field micrographs from regions with different dpa in the FG, UFG and NC G91 after irradiation at 300 °C. Images of the un-irradiated regions are also provided in Fig. 3. The corresponding dislocation loop size & density and dislocation line density at these locations in each sample are given in Fig. 4. For the FG G91, small dislocation loops (black dots), as well as dislocation lines, can be observed in the low dpa region near the irradiation surface. The loop and line density are $4.10 \times 10^{22} m^{-3}$ and $1.34 \times 10^{14} m^{-2}$, respectively, and the average size of the dislocation loop is 4.3 nm.

In the middle dpa region, a higher density of dislocation loops and lines are observed; some large loops up to 10 nm in size coexist with small loops, indicating that loop nucleation and growth occurred simultaneously. It is interesting to note that dislocation lines are often decorated by loops. Dislocation loop density and line density further increased to $8.29 \times 10^{22} m^{-3}$ and $1.78 \times 10^{14} m^{-2}$, respectively, in the high dpa regions. Further increases in dislocation loop density, dislocation line density and dislocation loop size are observed in the regions with the highest ion concentration. Note that arrays of dislocations appear beyond the damage regions, which could result from ion implantation. The dislocations were

Figure 3 Cross-section bright field STEM micrographs of FG (a1-4), UFG (b1-4) and NC (c1-4) G91 from low dpa, middle dpa, high dpa, and un-irradiated regions. Scale bar, 20 nm. All g vectors contributed to the image of the irradiated regions; the zone axis is indicated.

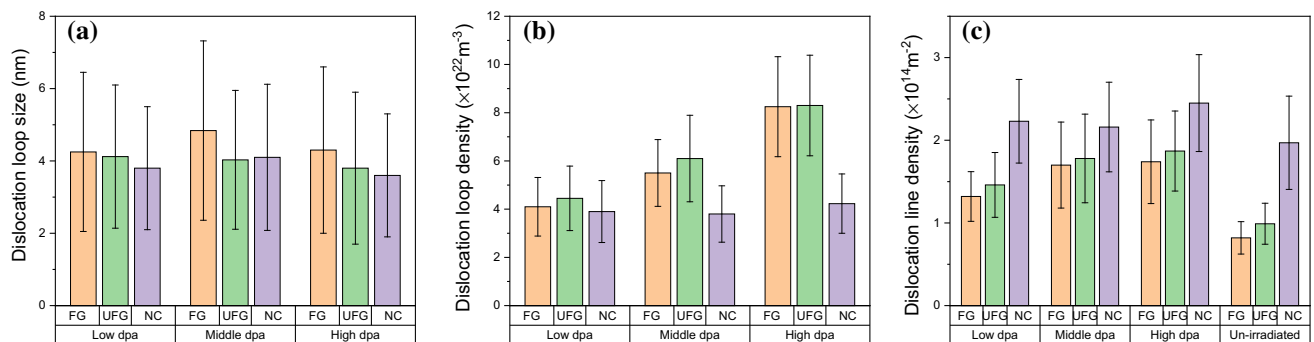
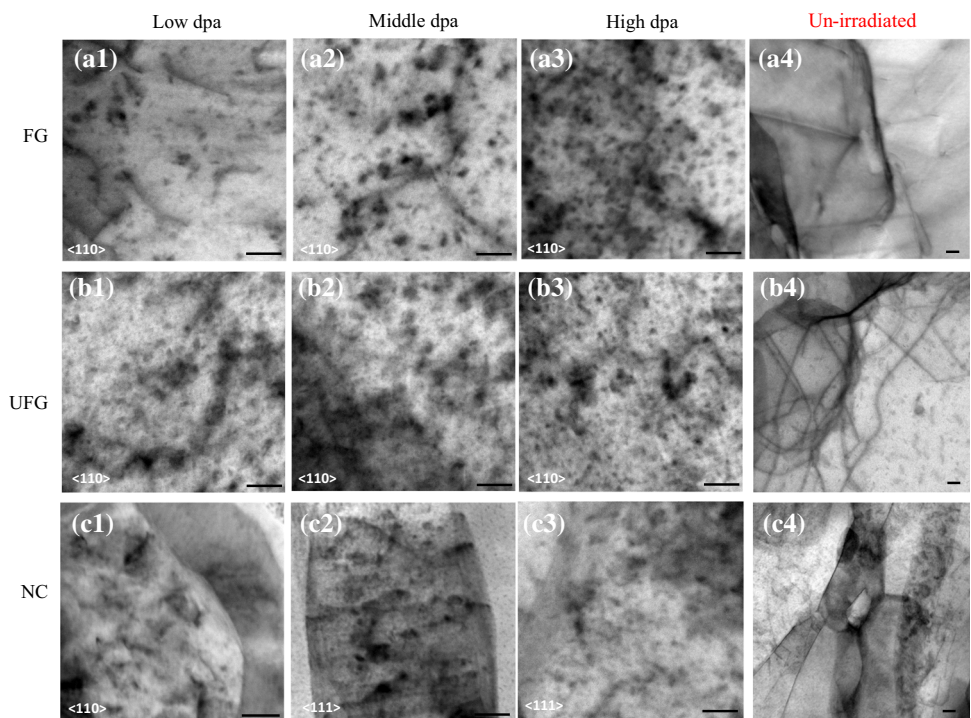


Figure 4 Measurements of the a dislocation loop size, b dislocation loop density and c dislocation line density in the FG, UFG and NC G91 steel samples from the low, middle and high dpa regions.

formed to accommodate the surface stresses induced by high doses of the implanted Fe [27]. For the UFG G91, the density of loops and dislocation lines near the surface is $4.50 \times 10^{22} m^{-3}$ and $1.46 \times 10^{14} m^{-2}$, respectively. As the damage level increases, the loop number density and line density increase. Our measurements indicate comparable increase in irradiation-induced defects in UFG and FG G91 when the dpa increases. For example, as the dpa increases from 30 (low dpa) to 100 (high dpa), the dislocation loop density and line density increase by 1.87 and 1.29 times, respectively, in UFG G91; in FG 91, the increases in loop and line density are 2.02 and 1.33 times, respectively. NC G91 exhibits a smaller dislocation loop density, i.e. $3.93 \times 10^{22} m^{-3}$, and a higher dislocation line density, i.e. $2.28 \times 10^{14} m^{-2}$ in the low dpa regions near the surface, as compared to the FG and UFG G91. Note that the UFG G91 appears to contain a larger number of defects compared to FG G91 in those scanning TEM (STEM) images; this is because the TEM lamella of UFG G91 is thicker, as confirmed by the EELS measurements. The higher dislocation line density found in the low dpa regions in NC G91 could be attributed to the higher strain introduced during HPT processing. The increase in irradiation damage in NC G91 was lower than those in FG and UFG G91 as dpa increases. The dislocation loop and line density only slightly increase to $4.23 \times 10^{22} m^{-3}$ and $2.45 \times 10^{14} m^{-2}$, respectively, in the high dpa regions. In addition, defects appear in the unirradiated regions of the UFG and NC G91 specimens. We would like to emphasize the challenges of making FIB specimens, especially for the HPT NC G91, due to the high residual strain. Therefore, FIB contamination and damages were more likely to be introduced to the NC G91 FIB specimens. Meanwhile, severe plastic deformation could also introduce defects before irradiation. Thus, the defects observed in NC G91 are not necessarily irradiation-induced. However, the NC G91 indeed shows much less difference in defect density across the depth than FG and UFG G91.

Void search was performed on the three variants of irradiated G91 steel samples in under-focus bright field. Some local voids with an average size of ~ 2.5 nm were found in larger grains of the FG G91 at a depth of 0.45–0.75 μm , as shown in Fig. 5. It is reasonable that the voids only appear in the middle dpa regions, as the high number of injected ions in the

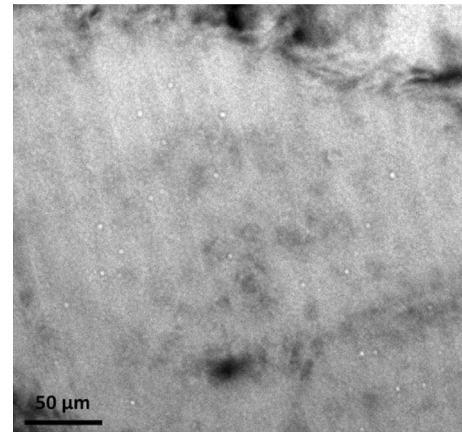


Figure 5 Bright field TEM image (defocus $-3 \mu m$) of FG G91, showing irradiation-induced voids in one grain.

high dpa regions and the high density of point defect sinks near the surface could suppress the void formation [28, 29]. In contrast, no voids were identified in UFG and NC G91.

Nano-indentation

Nano-indentations were carried out to monitor the changes in mechanical property in the irradiated regions. Figure 6 shows the nano-hardness (average and standard deviation in GPa) of the three variants of G91 steel samples irradiated at $300^\circ C$. Nano-hardness of the un-irradiated counterparts (masked during irradiation experiment) is also provided in Fig. 6 for comparison. For all the samples, the apparent hardness decreases with the indent displacement, which is the well-known indentation size effect (ISE). Results indicate that irradiated FG and UFG G91 exhibit notably higher hardness when compared to their un-irradiated counterparts. The irradiation-induced hardening, i.e. the hardness difference between the irradiated and un-irradiated condition, in the FG G91 is 1.7 GPa, 1.6 GPa and 1.4 GPa at 100 nm, 150 nm and 200 nm indent displacements, respectively. UFG G91 shows comparable irradiation hardening to FG G91. In contrast, the NC G91 exhibits negligible hardening after irradiation, with only 0.2 GPa and 0.4 GPa increases measured when indent displacements were 150 nm and 200 nm, respectively.

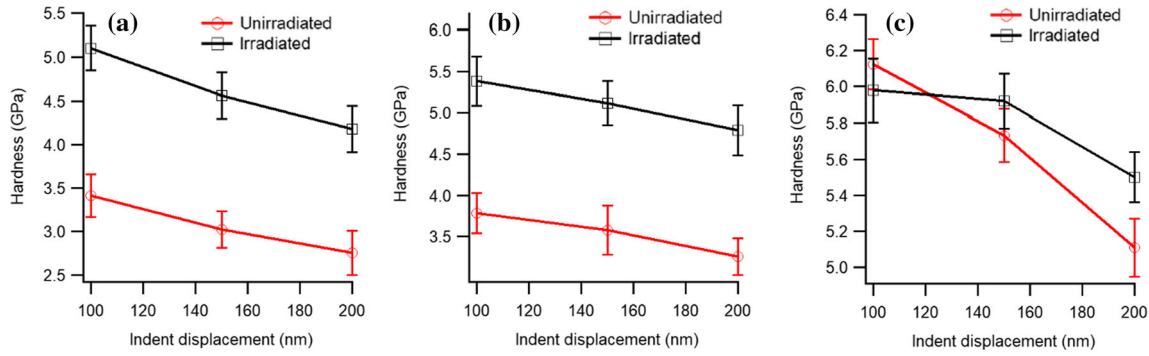


Figure 6 Comparison in hardness between the irradiated and un-irradiated regions at various indent displacements: **a** FG; **b** UFU; and **c** NC G91 irradiated with 3.7 MeV Fe ion at 300 °C.

Discussion

The irradiation experiments using Fe ion at 300 °C introduced damage up to 100 dpa to the three G91 steel variants of different grain size ranges. The comparisons in the irradiation damage among the three G91 steel variants were made, and the key findings are as follows:

1. Overall, NC G91 shows lower densities of irradiation-induced dislocation loops and lines when compared to FG and UFG G91.
2. The irradiation defect density vs. dose relationship is much less strong in NC G91 than in FG and UFG G91.
3. FG and UFG G91 showed measurable irradiation-induced hardening, whereas it was negligible in NC G91. This is attributed to the lower irradiation defect density in NC G91.
4. Voids were only identified in one grain in FG G91, whereas no voids were found in UFG and NC G91.

The results demonstrate that in current irradiation condition, NC G91 exhibits higher irradiation resistance than FG and UFG G91, which is discussed in more detail as follows.

Irradiation resistance

During ion irradiation, high-energy ions travel through the crystal and collide with lattice atoms, which are displaced as interstitials, leaving vacancies behind. The interstitials can travel and create more collisions, causing cascades. The interstitials and vacancies form various kinds of defect, e.g., dislocation loops, dislocation lines and voids, etc. GBs can

help to mitigate the damage via promoting defect recombination. GBs can act as neutral sinks that remove the defects by absorbing them and recombining interstitials-vacancies, and thus the irradiation damage is mitigated. In-situ irradiation experiments have provided the evidence for the efficacy of GBs absorbing the defects in various metals [15, 30, 31]. The sink strength of the GBs is estimated as $k_{gb}^2 = 60/d^2$, where d is the diameter of the grains and k_{gb} is the inverse of the average distance that a mobile defect can move before being absorbed by a GB. The effects of GBs on irradiation resistance have been studied in different alloys subjected to various irradiation conditions. In the current case, the k_{gb}^2 for NC ($d = 142$ nm, the average area-equivalent circular diameter) and FG G91 ($d = 610$ nm) is $3.0 \times 10^{15} m^{-2}$ and $1.6 \times 10^{14} m^{-2}$ respectively, indicating that the sink strength of NC G91 is 19 times greater than that of FG 91.

Dislocations were introduced during the severe plastic deformation processing (ECAP or HPT) of the G91 steel, which can also serve as defect sinks with a strength of $k_{dis}^2 = z_d \rho_d$, where ρ_d is the dislocation density and $z_d \sim 2-10$ is the number of the atomic sites on each of the crystallographic planes intersected by the dislocation line [6, 16]. Dislocation sink strength was estimated for FG and NC with $z_d = 6$. The dislocation densities in NC and FG G91 are measured as $1.96 \times 10^{14} m^{-2}$ and $0.867 \times 10^{14} m^{-2}$, respectively (data from the un-irradiated regions, Fig. 4c). The calculations indicate dislocation sink strength is $6.6 \times 10^{14} m^{-2}$ higher in NC than in FG G91, while GB sink strength is $28.4 \times 10^{14} m^{-2}$ higher in NC than in FG G91. It is concluded that the higher GB density in NC is the dominant reason for higher

irradiation resistance, although dislocations could add additional irradiation resistance to the NC G91. Note that dislocations are biased sinks with slight preference for interstitials over vacancies; however, when dislocation density is high enough, they can also provide many sink sites for vacancies, and thus the void nucleation and growth rate would also be suppressed [6].

It is noteworthy that FG and UFG G91 TEM lamellas exhibit similar density of defects, although the UFG G91 has a higher GB density. Possible explanations are provided here. Firstly, the grain size difference between FG and UFG G91 may not be enough to cause evident difference in irradiation resistance in the current irradiation conditions. Note that during the processing of G91, oil quenching was carried out to generate martensitic blocks, with the width of a few hundred micrometers; therefore, the G91 already exhibits fine structures even without ECAP. Only marginal benefit of mitigating irradiation damage was reported when Fe with ultra-fine grain sizes was subjected to 10 keV helium ion irradiation at 573 K [32]. Secondly, the characters of the GBs in the UFG G91 can affect the material's irradiation resistance. As reported [10], a high fraction of the GBs in the UFG G91 is low-angle GBs, which exhibit reduced sink strength than the high-angle GBs [33, 34]. Thus, finer grain sizes do not necessarily lead to significant improvement in irradiation resistance when a high fraction of the GBs are in low misorientations. Thirdly, post-irradiation annihilation may also be responsible for the negligible difference. After irradiation was completed, loops could still move to GBs or recombine during cooling. El-Atwani et al. [30] reported significant less dislocation loops in post-irradiation examination of a NC tungsten subjected to Kr ion irradiation to 2–10 dpa when compared to in-situ measurements; this was true even for room temperature irradiation. If indeed a larger number of defects were present during irradiation in FG G91 as compared to UFG G91, more defects would have the chance of being annihilated after irradiation stopped. Therefore, the final difference between FG and UFG G91 in irradiation-induced defects measured during the post-irradiation examination would be reduced.

The current results demonstrate that NC G91 has a higher radiation resistance than its UFG and FG counterparts. However, conclusion here may not necessarily be extended to extreme irradiation

conditions when the dose is up to hundreds of dpa. Gigax et al. [34] reported irradiation instability in ECAP processed UFG T91 at ultra-high damage levels, and reduced irradiation resistance of this material as compared to its coarse-grained counterpart at such high doses. As the dose increases, structural changes in GBs occur, i.e., high angle boundaries transformed to low angle boundaries, leading to a decline in the effectiveness of reducing irradiation damage. Also, voids become biased sinks for vacancies at extreme high dose, and grain growth is accelerated due to the biased absorption of interstitials by GBs. The irradiation behavior of NC G91 at ultra-high doses still needs to be investigated in the future.

Irradiation-induced hardening

Irradiation hardening results from irradiation-induced voids, precipitates, dislocation loops, dislocation lines, etc. For the current G91, voids were detected in one grain and only in irradiated FG G91; in addition, the density of the precipitates ($M_{23}C_6$ and MX, where M and X denote metallic elements and carbon and/or nitrogen, respectively) [9, 10] is comparable between the irradiated and un-irradiated regions. Therefore, contributions from voids and precipitates to the irradiation hardening are negligible, which is a reasonable assumption based on a previous irradiation study on the G91 [35]. The barrier hardening model is employed here to estimate the hardening, $\Delta\sigma_y$, from loops and dislocation lines:

$$\Delta\sigma_y = M\alpha_L Gb\sqrt{\rho_L d_L} + M\alpha_D Gb(\sqrt{\rho_D^{irr}} - \sqrt{\rho_D^{unirr}}) \quad (1)$$

where $M = 2.7$ is the Taylor factor for body-centered cubic materials, $G = 75\text{GPa}$ is the shear modulus of G91 steel at room temperature, $b = 0.25\text{nm}$ is the magnitude of the Burgers vector, α_L, ρ_L and d_L are the barrier strength, density and average size of the dislocation loops, respectively, and α_D, ρ_D^{unirr} and ρ_D^{irr} are the barrier strength of the dislocation lines and their density before and after irradiation, respectively. α_L and α_D here are taken as 0.40 and 0.64, respectively [35, 36]. The ρ_D^{unirr} values are measured to be $8.67 \times 10^{13} \text{ m}^{-2}$, $1.00 \times 10^{14} \text{ m}^{-2}$ and $1.96 \times 10^{14} \text{ m}^{-2}$ for the FG, UFG and NC G91, respectively. Based on the obtained statistics of the defects, estimation of the irradiation hardening using the empirical model was performed. The calculation results are displayed

Table 1 Comparison of measured hardening (from nano-indentation) and calculated hardening (via Eq. 1) in three G91 steel variants irradiated by Fe ion at 300 °C

	Measured hardening (MPa)	Calculated hardening (MPa)		
		Low dpa	Middle dpa	High dpa
FG	329 ± 70	340 ± 132	453 ± 181	518 ± 233
UFG	352 ± 59	345 ± 138	431 ± 182	484 ± 208
NC	94 ± 35	283 ± 107	282 ± 119	302 ± 119

in Table 1, indicating that: a) the FG and UFG overall exhibit higher hardening than the NC counterpart; b) as the dpa increases, the hardening increases in FG and UFG while it remains almost constant in the NC counterpart.

Nano-indentations were carried out to probe the mechanical property changes after irradiation in G91 with different microstructures. Generally, indentation should be no more than 10%–20% of the thickness of the interested region, so that the intrinsic properties of the interested region can be obtained and the interference from the underlying substrate can be avoided. Therefore, 200 nm is chosen as the reference depth for quantitative analyses of the hardness measurements. The nanoindentation results were first divided by 9.8 to convert to Vickers hardness numbers; then they were converted to Vickers hardness by multiplying a coefficient of 0.76, and further converted to yield strength by multiplying a coefficient of 3.06 [37–39]. The converted nano-indentation results are also presented in Table 1 for comparison. The values of the calculated hardening (e.g. from the low & middle dpa regions) via Eq. (1) are comparable to the measured hardening values via nano-indentation for FG and UFG G91. However, the calculations yield much higher hardening values than the measurement for NC G91. The discrepancy may be explained by two reasons. First, artifacts introduced during TEM sample preparation by FIB could be counted as irradiation-induced defects. It is difficult to entirely avoid any contamination and damage from FIB during sample preparation, although care was taken to minimize the damage from FIB. Second, the severe plastic deformation introduced defects before the irradiation [40, 41]. Both could lead to an over-estimation of the irradiation damage in HPT/NC G91.

In addition to GBs, the precipitate/matrix interfaces are also known as defect sinks that help to decrease the density of irradiation-induced dislocation loops [42–44]. G91 contains two types of precipitates, i.e., $M_{23}C_6$ and MX . Although severe plastic

deformation can significantly refine the grain size, it seems to have less impact on the size and fraction of those precipitates [10, 12]. Therefore, the improved irradiation resistance observed in NC G91 is not attributed to the precipitates.

Conclusions

Three G91 steel variants with different grain size ranges (FG, UFG and NC) were irradiated by Fe ion up to 100 dpa at 300 °C. The irradiation response of each variant was accessed. None of the three G91 steel variants exhibited irradiation-induced grain growth. Irradiation-induced voids were only found in FG G91. As the dpa rose along the irradiation depth, the density of the defects (dislocation loops and lines) increased; however, the increase rate was notably lower in NC G91 than in FG and UFG G91. Meanwhile, the NC G91 showed significantly lower irradiation hardening than FG and UFG G91. It is concluded that GBs effectively mitigate the irradiation damage when the microstructure is on the NC scale in G91 steel under the current irradiation condition.

Acknowledgements

This research was financially supported by the U.S. Department of Energy, Office of Nuclear Energy through the NEET-NSUF (Nuclear Energy Enabling Technology—Nuclear Science User Facility) program (award number DE-NE0008524), and through the NSUF-RTE program (award number 18-1403). Partial support for Haiming Wen and Andrew Hoffman came from the U.S. Nuclear Regulatory Commission (NRC) Faculty Development Program (award number NRC 31310018M0044). Ruslan Valiev gratefully acknowledges the financial support from Russian Foundation for Basic Research (Project 20-03-00614).

Declarations

Conflict of interest The authors declare that they have no known competing financial interests or personal relationships that could have appeared to influence the work reported in this paper.

References

- [1] Henry J, Maloy SA (2017) 9 - Irradiation-resistant ferritic and martensitic steels as core materials for Generation IV nuclear reactors. In: Yvon P (ed) Structural Materials for Generation IV Nuclear Reactors. Woodhead Publishing, pp 329–355
- [2] Bhattacharya A, Zinkle SJ (2020) 1.12 - Cavity Swelling in Irradiated Materials. In: Konings RJM, Stoller RE (eds) Comprehensive Nuclear Materials (Second Edition). Elsevier, Oxford, pp 406–455
- [3] Gaganidze E, Aktaa J (2013) Assessment of neutron irradiation effects on RAFM steels. *Fusion Eng Des* 88:118–128. <https://doi.org/10.1016/j.fusengdes.2012.11.020>
- [4] Zinkle SJ, Was GS (2013) Materials challenges in nuclear energy. *Acta Mater* 61:735–758. <https://doi.org/10.1016/j.actamat.2012.11.004>
- [5] Klueh RL, Harries DR (2001) High-chromium ferritic and martensitic steels for nuclear applications, in, AsTM West Conshohocken, PA,.
- [6] Was GS (2016) Fundamentals of radiation materials science: metals and alloys, springer.
- [7] Konstantinović MJ, Stergar E, Lambrecht M, Gavrilov S (2016) Comparison of the mechanical properties of T91 steel from the MEGAPIE, and TWIN-ASTIR irradiation programs. *J Nucl Mater* 468:228–231. <https://doi.org/10.1016/j.jnucmat.2015.07.038>
- [8] Yan H, Liu X, He L, Stubbins J (2021) Early-stage microstructural evolution and phase stability in neutron-irradiated ferritic-martensitic steel T91. *J Nucl Mater* 557:153207. <https://doi.org/10.1016/j.jnucmat.2021.153207>
- [9] Duan J, Wen H, Zhou C, He X, Islamgaliev R, Valiev R (2020) Annealing behavior in a high-pressure torsion-processed Fe–9Cr steel. *J Mater Sci* 55:7958–7968. <https://doi.org/10.1007/s10853-020-04560-3>
- [10] Duan J, Wen H, Zhou C, He X, Islamgaliev R, Valiev R (2019) Discontinuous grain growth in an equal-channel angular pressing processed Fe-9Cr steel with a heterogeneous microstructure. *Mater Characterization*. <https://doi.org/10.1016/j.matchar.2019.110004>
- [11] Duan J, Wen H, Zhou C, Islamgaliev R, Li X (2019) Evolution of microstructure and texture during annealing in a high-pressure torsion processed Fe-9Cr alloy. *Materialia* 6:100349. <https://doi.org/10.1016/j.mtla.2019.100349>
- [12] Duan J, He L, Fu Z, Hoffman A, Sridharan K, Wen H (2021) Microstructure, strength and irradiation response of an ultra-fine grained FeNiCoCr multi-principal element alloy. *J Alloy Compd* 851:156796. <https://doi.org/10.1016/j.jallcom.2020.156796>
- [13] Zhang X, Hattar K, Chen Y, Shao L, Li J, Sun C, Yu K, Li N, Taheri ML, Wang H, Wang J, Nastasi M (2018) Radiation damage in nanostructured materials. *Prog Mater Sci* 96:217–321. <https://doi.org/10.1016/j.pmatsci.2018.03.002>
- [14] Sun C, Song M, Yu KY, Chen Y, Kirk M, Li M, Wang H, Zhang X (2013) In situ evidence of defect cluster absorption by grain boundaries in Kr ion irradiated nanocrystalline Ni. *Metall and Mater Trans A* 44:1966–1974. <https://doi.org/10.1007/s11661-013-1635-9>
- [15] Chen D, Wang J, Chen T, Shao L (2013) Defect annihilation at grain boundaries in alpha-Fe. *Sci Rep* 3:1450. <https://doi.org/10.1038/srep01450>
- [16] Song M, Wu YD, Chen D, Wang XM, Sun C, Yu KY, Chen Y, Shao L, Yang Y, Hartwig KT, Zhang X (2014) Response of equal channel angular extrusion processed ultrafine-grained T91 steel subjected to high temperature heavy ion irradiation. *Acta Mater* 74:285–295. <https://doi.org/10.1016/j.actamat.2014.04.034>
- [17] Toloczko MB, Garner F, Voyevodin V, Bryk V, Borodin O, Mel'Nychenko V, Kalchenko A (2014) Ion-induced swelling of ODS ferritic alloy MA957 tubing to 500 dpa. *J Nucl Mater* 453:323–333. <https://doi.org/10.1016/j.jnucmat.2014.06.011>
- [18] Gigax J, Chen T, Kim H, Wang J, Price L, Aydogan E, Maloy SA, Schreiber D, Toloczko M, Garner F (2016) Radiation response of alloy T91 at damage levels up to 1000 peak dpa. *J Nucl Mater* 482:257–265. <https://doi.org/10.1016/j.jnucmat.2016.10.003>
- [19] Aydogan E, Chen T, Gigax J, Chen D, Wang X, Dzhumayev P, Emelyanova O, Ganchenkova M, Kalin B, Leontiva-Smirnova M (2017) Effect of self-ion irradiation on the microstructural changes of alloy EK-181 in annealed and severely deformed conditions. *J Nucl Mater* 487:96–104. <https://doi.org/10.1016/j.jnucmat.2017.02.006>
- [20] Was G, Jiao Z, Getto E, Sun K, Monterrosa A, Maloy S, Anderoglu O, Sencer B, Hackett M (2014) Emulation of reactor irradiation damage using ion beams. *Scripta Mater* 88:33–36. <https://doi.org/10.1016/j.scriptamat.2014.06.003>
- [21] Stoller RE (2002) The effect of free surfaces on cascade damage production in iron. *J Nucl Mater* 307:935–940. [https://doi.org/10.1016/S0022-3115\(02\)01096-6](https://doi.org/10.1016/S0022-3115(02)01096-6)
- [22] Weber WJ, Zhang Y (2019) Predicting damage production in monoatomic and multi-elemental targets using stopping and

- range of ions in matter code: Challenges and recommendations. *Curr Opin Solid State Mater Sci* 23:100757. <https://doi.org/10.1016/j.cossms.2019.06.001>
- [23] Stoller RE, Toloczko MB, Was GS, Certain AG, Dwaraknath S, Garner FA (2013) On the use of SRIM for computing radiation damage exposure. *Nucl Instrum Methods Phys Res, Sect B* 310:75–80. <https://doi.org/10.1016/j.nimb.2013.05.008>
- [24] Ziegler JF, Ziegler MD, Biersack JP (2010) SRIM – The stopping and range of ions in matter (2010). *Nucl Instrum Methods Phys Res, Sect B* 268:1818–1823. <https://doi.org/10.1016/j.nimb.2010.02.091>
- [25] Lin Y-R, Bhattacharya A, Chen D, Kai J-J, Henry J, Zinkle SJ (2021) Temperature-dependent cavity swelling in dual-ion irradiated Fe and Fe-Cr ferritic alloys. *Acta Mater* 207:116660. <https://doi.org/10.1016/j.actamat.2021.116660>
- [26] Egerton RF (2011) *Electron energy-loss spectroscopy in the electron microscope*, Springer Science & Business Media.
- [27] Didenko AN, Kozlov EV, Sharkeev YP, Tailashev AS, Rjabchikov AI, Pranjavichus L, Augulis L (1993) Observation of deep dislocation structures and “long-range effect” in ion-implanted α -Fe. *Surf Coat Technol* 56:97–104. [https://doi.org/10.1016/0257-8972\(93\)90012-D](https://doi.org/10.1016/0257-8972(93)90012-D)
- [28] Shao L, Wei CC, Gigax J, Aitkaliyeva A, Chen D, Sencer BH, Garner FA (2014) Effect of defect imbalance on void swelling distributions produced in pure iron irradiated with 3.5MeV self-ions. *J Nucl Mater* 453:176–181. <https://doi.org/10.1016/j.jnucmat.2014.06.002>
- [29] Sun C, Garner FA, Shao L, Zhang X, Maloy SA (2017) Influence of injected interstitials on the void swelling in two structural variants of 304L stainless steel induced by self-ion irradiation at 500°C. *Nucl Instrum Methods Phys Res, Sect B* 409:323–327. <https://doi.org/10.1016/j.nimb.2017.03.070>
- [30] El-Atwani O, Esquivel E, Aydogan E, Martinez E, Baldwin JK, Li M, Uberuaga BP, Maloy SA (2019) Unprecedented irradiation resistance of nanocrystalline tungsten with equiaxed nanocrystalline grains to dislocation loop accumulation. *Acta Mater* 165:118–128. <https://doi.org/10.1016/j.actamat.2018.11.024>
- [31] El-Atwani O, Esquivel E, Efe M, Aydogan E, Wang YQ, Martinez E, Maloy SA (2018) Loop and void damage during heavy ion irradiation on nanocrystalline and coarse grained tungsten: Microstructure, effect of dpa rate, temperature, and grain size. *Acta Mater* 149:206–219. <https://doi.org/10.1016/j.actamat.2018.02.035>
- [32] El-Atwani O, Nathaniel JE, Leff AC, Hattar K, Taheri ML (2017) Direct observation of sink-dependent defect evolution in nanocrystalline iron under irradiation. *Sci Rep* 7:1836. <https://doi.org/10.1038/s41598-017-01744-x>
- [33] Han WZ, Demkowicz MJ, Fu EG, Wang YQ, Misra A (2012) Effect of grain boundary character on sink efficiency. *Acta Mater* 60:6341–6351. <https://doi.org/10.1016/j.actamat.2012.08.009>
- [34] Gigax JG, Kim H, Chen T, Garner FA, Shao L (2017) Radiation instability of equal channel angular extruded T91 at ultra-high damage levels. *Acta Mater* 132:395–404. <https://doi.org/10.1016/j.actamat.2017.04.038>
- [35] Liu X, Miao Y, Li M, Kirk MA, Maloy SA, Stubbins JF (2017) Ion-irradiation-induced microstructural modifications in ferritic/martensitic steel T91. *J Nucl Mater* 490:305–316. <https://doi.org/10.1016/j.jnucmat.2017.04.047>
- [36] Bergner F, Pareige C, Hernández-Mayoral M, Malerba L, Heintze C (2014) Application of a three-feature dispersed-barrier hardening model to neutron-irradiated Fe–Cr model alloys. *J Nucl Mater* 448:96–102. <https://doi.org/10.1016/j.jnucmat.2014.01.024>
- [37] Yabuuchi K, Kuribayashi Y, Nogami S, Kasada R, Hasegawa A (2014) Evaluation of irradiation hardening of proton irradiated stainless steels by nanoindentation. *J Nucl Mater* 446:142–147. <https://doi.org/10.1016/j.jnucmat.2013.12.009>
- [38] Chen D, Murakami K, Dohi K, Nishida K, Li Z, Sekimura N (2020) The effects of loop size on the unfaulting of Frank loops in heavy ion irradiation. *J Nucl Mater*. <https://doi.org/10.1016/j.jnucmat.2019.151942>
- [39] Busby JT, Hash MC, Was GS (2005) The relationship between hardness and yield stress in irradiated austenitic and ferritic steels. *J Nucl Mater* 336:267–278. <https://doi.org/10.1016/j.jnucmat.2004.09.024>
- [40] Setman D, Kerber MB, Schafler E, Zehetbauer MJ (2010) Activation enthalpies of deformation-induced lattice defects in severe plastic deformation nanometals measured by differential scanning calorimetry. *Metall and Mater Trans A* 41:810–815. <https://doi.org/10.1007/s11661-009-0058-0>
- [41] Setman D, Schafler E, Korznikova E, Zehetbauer MJ (2008) The presence and nature of vacancy type defects in nanometals detained by severe plastic deformation. *Mater Sci Eng, A* 493:116–122. <https://doi.org/10.1016/j.msea.2007.06.093>
- [42] Zhao MZ, Liu PP, Bai JW, Zhu YM, Wan FR, Ohnuki S, Zhan Q (2014) In-situ observation of the effect of the precipitate/matrix interface on the evolution of dislocation structures in CLAM steel during irradiation. *Fusion Eng Des* 89:2759–2765. <https://doi.org/10.1016/j.fusengdes.2014.07.022>
- [43] Getto E, Vancoervering G, Was GS (2017) The co-evolution of microstructure features in self-ion irradiated HT9 at very high damage levels. *J Nucl Mater* 484:193–208. <https://doi.org/10.1016/j.jnucmat.2016.12.006>

- [44] Liu PP, Zhao MZ, Zhu YM, Bai JW, Wan FR, Zhan Q (2013) Effects of carbide precipitate on the mechanical properties and irradiation behavior of the low activation martensitic steel. *J Alloy Compd* 579:599–605. <https://doi.org/10.1016/j.jallcom.2013.07.085>

Publisher's Note Springer Nature remains neutral with regard to jurisdictional claims in published maps and institutional affiliations.